International Journal of Biological Macromolecules 181 (2021) 313–321

Contents lists available at ScienceDirect

International Journal of Biological Macromolecules

journal homepage: http://www.elsevier.com/locate/ijbiomac

Facile fabrication and characterization of kraft lignin@Fe_3O_4 nanocomposites using pH driven precipitation: Effects on increasing lignin content

Frankie A. Petrie [a], Justin M. Gorham [b], Robert T. Busch [a], Serhiy O. Leontsev [c], Esteban E. Ureña-Benavides [d], Erick S. Vasquez [a,e,*]

[a] Department of Chemical and Materials Engineering, University of Dayton, 300 College Park, Dayton, OH 45469-0256, USA
[b] Materials Measurement Science Division, National Institute of Standards and Technology, 100 Bureau Dr., Gaithersburg, MD 20899, USA
[c] UES, Inc., 4401 Dayton-Xenia Rd., Dayton, OH 45432, USA
[d] Department of Biomedical Engineering and Chemical Engineering, The University of Texas at San Antonio, One UTSA Circle, San Antonio, TX 78249, USA
[e] Integrative Science and Engineering Center, University of Dayton, 300 College Park, Dayton, OH 45469, USA

ARTICLE INFO

Article history:
Received 14 January 2021
Received in revised form 5 March 2021
Accepted 13 March 2021
Available online 22 March 2021

Keywords:
Fe_3O_4
Kraft lignin
Lignin@Fe_3O_4 nanocomposites

ABSTRACT

This work offers a facile fabrication method for lignin nanocomposites through the assembly of kraft lignin onto magnetic nanoparticles (Fe_3O_4) based on pH-driven precipitation, without needing organic solvents or lignin functionalization. Kraft lignin@Fe_3O_4 multicore nanocomposites fabrication proceeded using a simple, pH-driven precipitation technique. An alkaline solution for kraft lignin (pH 12) was rapidly injected into an aqueous-based Fe_3O_4 nanoparticle colloidal suspension (pH 7) under constant mixing conditions, allowing the fabrication of lignin magnetic nanocomposites. The effects of increasing lignin to initial Fe_3O_4 mass content (g/g), increasing in ratio from 1:1 to 20:1, are discussed with a complete chemical, structural, and morphological characterization. Results showed that nanocomposites fabricated above 5:1 lignin:Fe_3O_4 had the highest lignin coverage and content (>20%), possessed superparamagnetic properties ($Ms \approx 45{,}000\ A \cdot m^2/kg^2$); had a negative surface charge (−30 mV), and formed multicore nanostructures ($D_H \approx 150$ nm). The multicore lignin@Fe_3O_4 nanocomposites allowed rapid magnetically induced separations from suspension. After 5 min exposure to a rare-earth neodymium magnet (1.27 mm × 1.27 mm × 5.08 mm), lignin@Fe_3O_4 nanocomposites exhibited a maximum methylene blue removal efficiency of 74.1% ± 7.1%. These nanocomposites have potential in magnetically induced separations to remove organic dyes, heavy metals, or other lignin adsorbates.

1. Introduction

Lignin is a high-value, underutilized macromolecule with unique properties, making it an attractive material for multifunctional structures ranging from the nano- to the macroscopic scale [1,2]. This biomacromolecule has been used to prepare antioxidant and UV adsorbent materials, antimicrobial agents, polymer-metal nanocomposites, and reinforced polymer blends [3,4]; however, only ≈2% of lignin is recovered and used in value-added products or applications [5]. An increase in lignin valorization could result from efficient methods to prepare lignin nanoparticles or nanocomposites. These have proven potential as protein vehicles for biomedical applications, templates to prepare hollow particles, and coatings to prevent degradation, oxidation, or dehydration of polymeric- and metal oxide particles [6–8].

Traditional synthetic routes for lignin nanoparticles include solvent evaporation, sonication and mechanical shearing, and crosslinking reactions [9]. Recent efforts demonstrated antisolvent-driven techniques as efficient, economical, and simple methods to prepare lignin nanoparticles [10,11]. The antisolvent-induced nanomaterial formation proceeds by merely adding a lignin solution in a good solvent into a poor solvent, or vice versa [12–17]. Nanoparticle properties are often controlled by adjusting experimental conditions such as the injection rate of the poor solvent [7], the total concentration of the initial lignin solution [18], or solution pH [19]. Once lignin nanoparticles are prepared, the preparation of nanocomposites proceeds by including other types of materials such as polymers or metallic nanoparticles.

The addition of magnetic nanoparticles to lignin imparts additional features allowing its manipulation in suspension by an external magnetic field. Magnetite, Fe_3O_4, is commonly used in nanocomposites due to its biocompatibility, stability in different physiological conditions, high magnetic saturation, superparamagnetic properties, and tunability in shape and dimensions [20]. Using lignin as a coating of

* Corresponding author at: Department of Chemical and Materials Engineering, University of Dayton, 300 College Park, Dayton, OH 45469-0256, USA.
E-mail address: evasquez1@udayton.edu (E.S. Vasquez).

https://doi.org/10.1016/j.ijbiomac.2021.03.105
0141-8130/

Fe_3O_4 results in a highly adsorptive nanocomposite with magnetic properties that can ultimately be used for many separation processes, from environmental to biological applications [21–30]. Unfortunately, the current fabrication methods for the preparation of lignin-magnetic nanocomposites require lignin chemical functionalization protocols [22,31] or numerous solvents and purification steps [26,32]. Only a few reports have analyzed the chemical, morphological, and magnetic properties of lignin magnetic nanocomposites based on the fabrication method to the authors' knowledge. Understanding these properties as a function of preparation conditions is key to an optimized synthesis that can facilitate large-scale production.

This work aims to provide a facile fabrication technique to prepare lignin magnetic nanocomposites based on the rapid injection of a lignin aqueous solution—initially dissolved at a pH 12—into a colloidal suspension of Fe_3O_4 magnetic nanoparticles dispersed in water (pH 7) under constant mixing conditions. Due to its proven dissolution in alkaline solutions above pH 10 [33] and large availability [5], kraft lignin was chosen. The precipitation and assembly of lignin onto the as-prepared magnetic nanoparticles suspended in water occur by merely adjusting the pH from alkaline to neutral conditions, eliminating the need for organic solvents such as ethanol or tetrahydrofuran (THF), found in antisolvent-induced precipitation. This procedure results in the assembly of kraft lignin coated magnetic nanocomposites (lignin@Fe_3O_4), which possess a unique multicore structure where multiple Fe_3O_4 crystals are encapsulated within the kraft lignin shell [34]. These multicore, heterogeneous lignin nanostructures are attractive due to improved magnetically driven separation with low magnetic fields.

The study also examines the effects of increasing kraft lignin content on the assembly of lignin@Fe_3O_4 nanocomposites at five different mass ratios of lignin to Fe_3O_4: 1:1, 5:1, 10:1, 12.5:1, and 20:1. Lignin@Fe_3O_4 nanocomposites assembly through the pH-driven precipitation technique is confirmed through the following: 1) the chemical characterization using X-ray diffraction (XRD), Fourier transform infrared (FTIR) spectroscopy, and X-ray photoelectron spectroscopy (XPS); 2) the lignin coating content using thermogravimetric analysis (TGA); 3) the morphological features using transmission electron microscopy (TEM) imaging and stability in suspension with dynamic light scattering (DLS) and ζ-potential measurements; and 4) the magnetic properties using superconducting quantum interference device (SQUID) measurements, and demonstrated separation of methylene blue by using only a rare-earth magnet and the lignin@Fe_3O_4 nanocomposites.

2. Experimental section[1]

Note: Additional details for the synthesis and characterization of the lignin@Fe_3O_4 nanocomposites (Sections 2.2–2.6) can be found in the supporting information (SI).

2.1. Materials

Iron (II) chloride (98%), iron (III) chloride (97%), ammonium hydroxide solution (28.0% to 30.0%), and kraft lignin ($M_w \approx 10{,}000$ u), the lignin type used throughout this study, were supplied by Sigma-Aldrich (St. Louis, MO, USA). Methylene blue (pure, certified) was supplied by Acros Organics (Fair Lawn, NJ). Ultrapure water with 18.2 MΩ-cm resistivity was obtained from an Elga PURELAB (UK) system and used for all experiments. All chemicals were used as received without further purification.

[1] Certain commercial entities, equipment, or materials may be identified in this document in order to describe an experimental procedure or concept adequately. Such identification is not intended to imply recommendation or endorsement by the National Institute of Standards and Technology, nor is it intended to imply that the entities, materials, or equipment are necessarily the best available for the purpose.

2.2. Synthesis of Fe_3O_4 magnetic nanoparticles

The synthesis of Fe_3O_4 magnetic nanoparticles was based on Massart's method with slight modifications [35], which can be found in the SI. In brief, iron (II) chloride solution was mixed with iron (III) chloride solution in a nitrogen-purged vessel at room temperature and then heated to 60 °C for 30 min. Magnetic nanoparticles were formed using 1 mol/L ammonium hydroxide solution added by syringe pump and separation of the black precipitate formed was achieved using an external magnet. The precipitate was washed in triplicate with water and stored at a final pH of 7.2 ± 0.2.

2.3. Fabrication and assembly of lignin@Fe_3O_4 nanocomposites

Kraft lignin was dissolved in an aqueous ammonium hydroxide solution (volume fraction of 5% or $\varphi_{NH_4OH} = 5\%$) at a concentration of 0.1 g/mL (pH = 12.3). The assembly of kraft lignin onto Fe_3O_4 nanoparticles proceeded by rapidly injecting the lignin solution into the Fe_3O_4 colloidal suspension at injection rates of 15–30 mL/min using a syringe pump, as shown in Scheme 1. Five conditions were studied at the following theoretical lignin to Fe_3O_4 mass ratios: 1:1, 5:1, 10:1, 12.5:1, 20:1 [SI, please refer to Table S1 for specific details]. After the rapid lignin solution injection, each colloidal suspension was mixed for 30 min at ≈17 Hz using an overhead stirrer followed by a centrifugation step at ≈417 Hz for 15 min. The supernatant was removed, and the solid precipitate was washed with water and sonicated in an ultrasonic bath for 20 min. This washing process was repeated three times, followed by the re-dispersion of the lignin@Fe_3O_4 in water. The final pH of the lignin@Fe_3O_4 suspension was 7.2 ± 0.2.

2.4. Chemical characterization of lignin@Fe_3O_4 nanocomposites

A Nicolet iS50 FTIR spectrophotometer (Madison, WI) with an iS50 MCT-A liquid nitrogen cooled detector with a CdTe window and a Smart Golden Gate ZnSe Attenuated total reflectance (ATR) accessory was used for ATR-FTIR data collection. Each spectrum was taken three times, and all data presented is an average of the values for the three spectra plus or minus the standard error of the mean. Please see SI for more information on sample preparation and analysis details.

XRD data were collected using a Rigaku SmartLab XRD instrument (The Woodlands, TX) with Cu K-alpha radiation at 40 kV and a current setting of 44 mA (please see SI for more details). The Scherrer Eq. (1) was used to determine the crystallite size "τ" using the most intense XRD peak at 35°, where K is the shape factor (0.9), λ is the wavelength (0.15418 nm), β is the full width at half maximum (FWHM), and θ is the Bragg diffraction angle.

$$\tau = \frac{K\lambda}{\beta \cos(\theta)} \quad (1)$$

XP spectra were acquired on an Axis Ultra DLD spectrometer from Kratos Analytical (Chestnut Ridge, NY) using monochromatic Al Kα X-rays operating at 150 W (10 mA; 15 kV) under ultra-high vacuum system ($P_{base} \approx 6.6 \times 10^{-8}$ Pa) conditions. After surface neutralization, spectra were acquired using a pass of 40 eV with photoelectron intensity measured in 0.1 eV steps in elemental regions of interest. Unless otherwise mentioned, all spectra were (A) processed and analyzed using CasaXPS software (Teignmouth, UK), (B) fit with a Shirley background, and (C) charge referenced to 530.1 eV consistent with O 1s for iron oxide particles [36]. All elements were corrected using elemental relative sensitivity factors provided by the manufacturer. Unless otherwise stated, the semi-quantitative XPS values represent the average of four spatially unique measurements from one sample with the standard deviation representing the heterogeneity of that sample [Please see the SI for additional details on sample preparation, measurement conditions, and analysis].

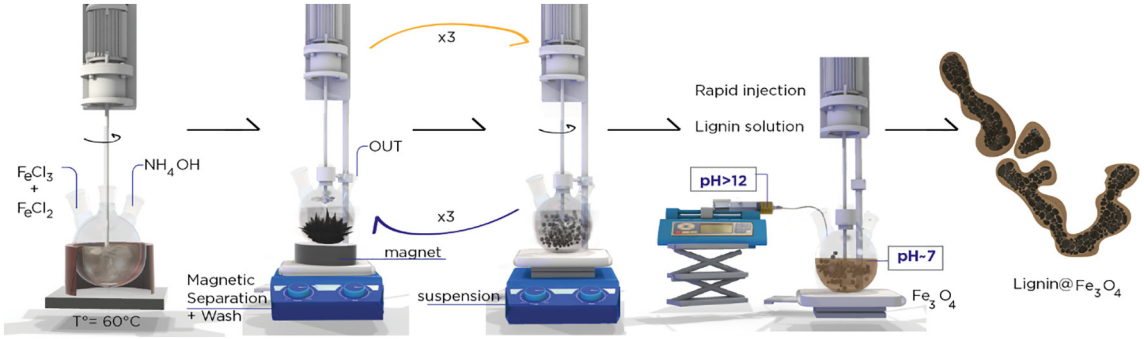

Scheme 1. Fabrication scheme for the facile preparation of lignin@Fe_3O_4 nanocomposites using pH-induced precipitation of kraft lignin (pH >12) injected into a colloidal iron oxide suspension (pH ≈ 7) at a high injection rate and mixing speed.

2.5. Lignin coating percentage, morphology, DLS and zeta-potential measurements of lignin@Fe_3O_4 nanocomposites

Thermogravimetric analysis (TGA) was performed using a TA Instruments TGA Q500 analyzer (New Castle, DE). The powdered nanoparticles (≈6 mg) were placed onto a platinum pan, and the tests were run under nitrogen flow at a flow rate of 10 mL/min and a temperature range of 25 °C to 900 °C. A constant heating rate of 10 °C/min was used. At each lignin:Fe_3O_4 mass ratio, measurements were obtained from unique reaction batches. The percent lignin content calculated is the average of at least three independent runs.

A Hitachi H-7600 TEM was used to visualize the nanoparticle morphologies, and it was operated at an accelerating voltage of 100 kV. The size of the Fe_3O_4 nanoparticles was calculated with ImageJ processing. The average particle size is reported from fifteen separate TEM images of each lignin:Fe_3O_4 mass ratio discussed. A NanoBrook 90Plus (BIC, Holtsville, NY) with a 40 mW, 640 nm temperature-controlled diode laser was used for DLS data collection. ζ-Potential measurements were collected using an Anton Paar Litesizer 500 instrument (Graz, Austria) that has a 40 mW, 658 nm laser. For both DLS and ζ-potential measurements, each trial was run at least in triplicate, collected at 25 °C, and the average results with a standard deviation is reported.

2.6. Lignin@Fe_3O_4 nanocomposites: magnetic properties and magnetically-induced separation of methylene blue

The magnetic moment of the lignin@Fe_3O_4 nanocomposites was measured at room temperature in the range of applied DC field of −3 T to 3 T using a Quantum Design XL superconducting quantum interference device (SQUID) magnetometer (San Diego, CA) (please see SI, for instrumental capabilities and parameters). Lignin@Fe_3O_4 powder samples were placed in size four snap-fit gel capsules (TedPella, Inc., Redding, CA) for analysis in the instrument with a minimum powder amount of 50 mg. Measured saturation magnetic moment values normalized by sample mass were used to compare lignin mass fractions between the nanocomposite samples.

A Perkin-Elmer Lambda 900 UV–Vis/NIR spectrometer (Waltham, MA) was used to analyze methylene blue (MB) adsorption by the fabricated lignin@Fe_3O_4 nanocomposites at the different lignin to Fe_3O_4 mass ratios. A stock solution of 7.2×10^{-3} mg/mL MB was prepared, and a UV–Vis spectrum was collected. 3 mg of each lignin@Fe_3O_4 type were placed in a vial and combined with 3 mL of the stock MB solution, sonicated for 3 min. Next, the vial was placed beside a neodymium magnet (1.77 cm × 1.77 cm × 5.08 cm; Applied Magnets, Plano, TX) for 5 min to separate the lignin@Fe_3O_4 nanoparticles. The remaining solution was then removed via pipette and ran through UV–Vis to determine the amount of non-adsorbed MB. Each sample was run in triplicate, including the stock solution.

2.7. Statistical analysis

Quantitative data are expressed as the mean ± standard deviation/error of the mean and noted in figure captions for each experimental result. TGA and DLS data and methylene blue adsorption studies were analyzed using one-way analysis of variance (ANOVA) to confirm the statistical difference. All data, and additional statistical tests, were processed using JMP Pro v.14 by the SAS Institute or OriginPro v.2020b by the OriginLab corporation.

3. Results and discussion

3.1. Chemical characterization of lignin and lignin@Fe_3O_4 nanocomposites

The Fe_3O_4, kraft lignin, and the lignin@Fe_3O_4 nanocomposites were chemically characterized by ATR-FTIR, XRD, and XPS. For Fe_3O_4, the FTIR spectrum (Fig. 1A) had two peaks, one at 3382 cm^{-1} representative of -OH stretching and one at 1636 cm^{-1}, which indicated O—H scissoring. Compared to the original water spectra, the 3382 cm^{-1} peak was red-shifted slightly, while the 1636 cm^{-1} was indicative of water interacting with a surface—generally an oxide group—and had been posited as water molecules forming hydrogen bonds to the Fe_3O_4 [37]. For kraft lignin, the FTIR spectrum (Fig. 1A) revealed several peaks in the 1750 cm^{-1} to 1000 cm^{-1} range [38,39]. The peak identified at 1040 cm^{-1} is associated with C—O deformation. The peak at 1120 cm^{-1} was assigned to the aromatic C—H deformation. The band at 1220 cm^{-1} was identified as C—C, C—O, or C═O stretching. The peak at 1380 cm^{-1} was attributed to C—C stretching. The peaks identified at 1450 cm^{-1}, 1510 cm^{-1}, 1590 cm^{-1} corresponded to the C═C stretching of aromatic bonds, C—C stretching of aromatic bonds, and the aromatic vibrations, respectively. The band at 1650 cm^{-1} represented the conjugated carboxyl group, and the peak at 2950 cm^{-1} is related to the stretching vibrations of C—H bonds [7].

The FTIR spectra of the lignin@Fe_3O_4 nanocomposites contained many of the same peaks as neat kraft lignin, confirming the successful formation of the conjugate system. Fig. 1A shows the lignin@Fe_3O_4 nanoparticles prepared at a 10:1 lignin:Fe_3O_4 mass ratio. As observed, there was a blueshift of ≈10 cm^{-1} on the peak at 1650 cm^{-1} for the lignin@Fe_3O_4. This shift was attributed to the hydrogen bonding between -OH groups on the Fe_3O_4 and the -OH groups on lignin [24,40]. Due to the large number of interactions occurring within the lignin structure, this shift may be caused by structural changes within the lignin during the binding procedure, including π-π interactions [37]. The peaks at 1120 cm^{-1}, 1380 cm^{-1}, and 1590 cm^{-1} attributed to the C—H deformation, C—C stretching, and aromatic vibrations, respectively, had a lower signal intensity for the lignin@Fe_3O_4. Note that few lignin peaks were found in the 1:1 mass ratio of lignin to Fe_3O_4 spectrum, which were in a closer agreement to the uncoated nanoparticle spectrum

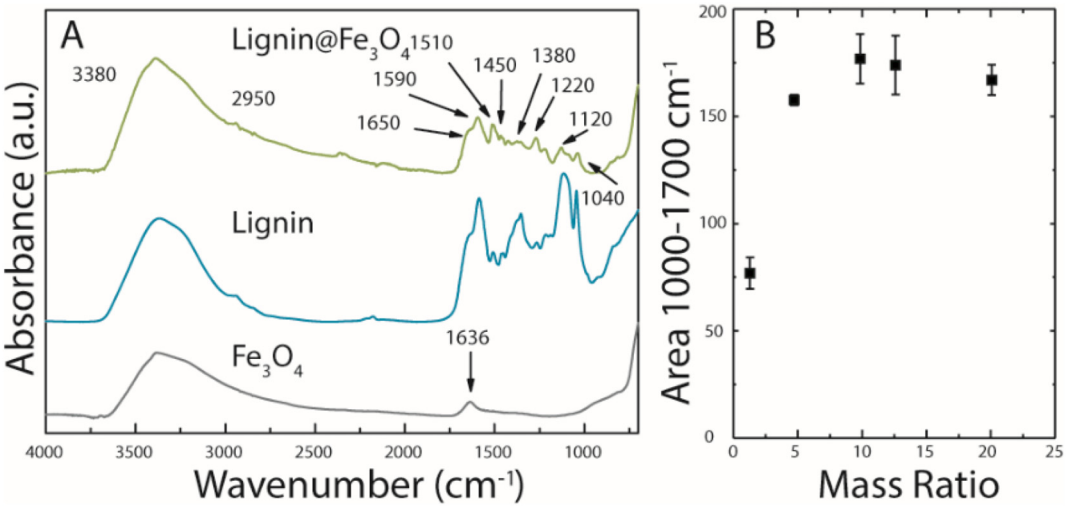

Fig. 1. (A) ATR-FTIR spectra of Fe_3O_4, neat kraft lignin, and lignin@Fe_3O_4 nanocomposites prepared at a 10:1 lignin:Fe_3O_4 mass ratio. (B) Integrated absorbance in the 1000 cm^{-1} to 1700 cm^{-1} region for each lignin@Fe_3O_4 nanocomposites as a function of lignin to Fe_3O_4 mass ratio, normalized to the 3380 cm^{-1} peak before integration. Results are the average ± the standard error from triplicate measurements.

[Fig. S1A], consistent with the notion that less lignin coated the nanoparticles at this condition than at higher mass ratios. For all other samples, the IR peaks corresponding to lignin were observed [SI; Fig. S1B and Table S2].

The signal intensity of the 1000 cm^{-1} to 1700 cm^{-1} region was integrated to represent the relative amount of lignin adsorption at the various mass ratios. There are no reported contributions from the Fe_3O_4 surface in this region, and the results are shown in Fig. 1B. The integrated absorbance exhibited logarithmic growth with increasing mass ratio, achieving saturation near the 5:1 mass ratio. The 10:1 had the highest absorbance ratio; however, no significant statistical differences were found for ratios greater than 5:1. Hence through FT-IR analysis, at or above this ratio, no differences were found on the highest achievable lignin content on the lignin@Fe_3O_4 nanocomposites.

XRD patterns for Fe_3O_4 were collected as a reference before adding any amount of the lignin. Primary Bragg reflections were identified at 2-theta of 30°, 35°, 43°, 53°, 57°, and 63°. The Miller indices were identified at these positions and are shown in Fig. 2, (220), (311), (400), (422), (511), and (440), indicating that the structure is a face-centered cubic lattice. These results matched previous literature values on Fe_3O_4 [41,42]. In addition, Fig. 2 shows XRD profiles for each of the lignin@Fe_3O_4 nanocomposites prepared at each mass ratio and compared to the uncoated Fe_3O_4 nanoparticles. These results showed no changes in composition of the Fe_3O_4 core upon the addition of the lignin coating. The average size of the neat Fe_3O_4 was 10.0 nm ± 1.9 nm, based on Eq. (1), for the Fe_3O_4, which is within range of reported crystallite sizes prepared using co-precipitation methods [41,43,44]. Note that the lignin@Fe_3O_4 nanocomposites had an initial increase in crystallite size at the 1:1 ratio of 16.2 nm ± 0.4 nm before converging near original crystallite size of 10.3 nm ± 0.8 nm by the 10:1 sample (Fig. S2). The increase of crystallite size at low lignin ratios (1:1 and 5:1) was likely due to lowered concentration of available kraft lignin capping agents during pH precipitation, resulting in a decreased ability to form a lignin coating, as previously discussed for coated maghemite particles [45].

XPS was employed to evaluate the relative elemental and chemical changes in the lignin@Fe_3O_4 nanocomposites as a function of mass ratio. Fig. 3 provides representative spectra from select lignin@Fe_3O_4 specimens (lignin:Fe_3O_4 = 0, 1, and 10; Fig. S3 for all mass ratios). The Fe 2p spectra had a peak maximum at 710.6 eV ± 0.2 eV (average and standard deviation of 24 Fe measurements) with an observable satellite feature between 718 eV and 719.5 eV. This line shape more closely resembled Fe_2O_3 than Fe_3O_4 [46], suggesting that at least some nanoparticle oxidation occurred post-synthesis. Indeed, previous reports have shown that non-stoichiometric Fe_3O_4 also results in the appearance of the Fe^{3+} satellite due to the loss of the Fe^{2+} satellite from FeO [36,47]. The O 1s spectra were fit with three different oxygen features at 530.1 eV ± 0.0 eV (*O-1*: representative of the O—Fe peak), 531.2 eV ± 0.1 eV (*O-2*: attributed to both the nanoparticle and lignin), and 533.1 eV ± 0.1 eV (*O-3*: representative of O—C from lignin) (positions are the average and standard deviation of 5 lignin@Fe_3O_4 specimens; please see the SI for further analysis/fitting details). As is evident from Fig. 3, *O-3* was especially useful as it can be employed to monitor the adsorption of the lignin to the surface of the Fe_3O_4 nanoparticle surface. XPS results for the nanocomposites prepared in this work did not show evidence for a covalent bond between the kraft lignin and the Fe_3O_4 nanoparticles.

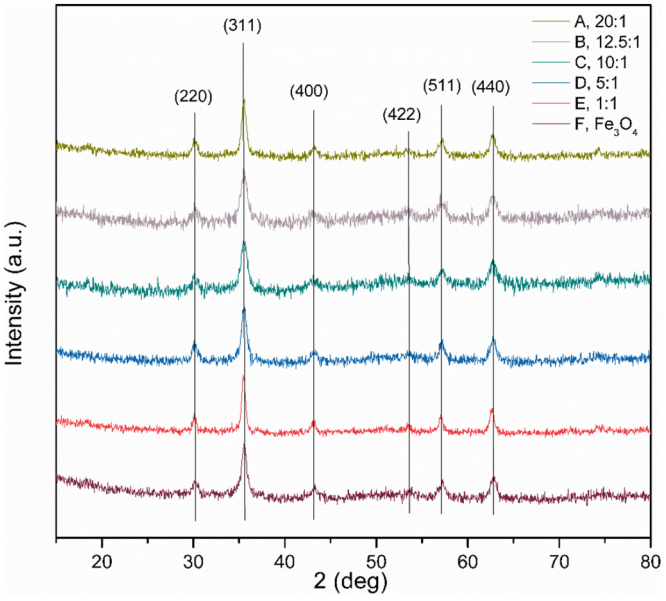

Fig. 2. Normalized XRD spectra for the five mass ratios of lignin@Fe_3O_4 nanocomposites and neat Fe_3O_4, identifying the Miller indices and Bragg reflections. The lignin coating amount had a negligible impact on the Fe_3O_4 peaks. [Results are from one sample measurement].

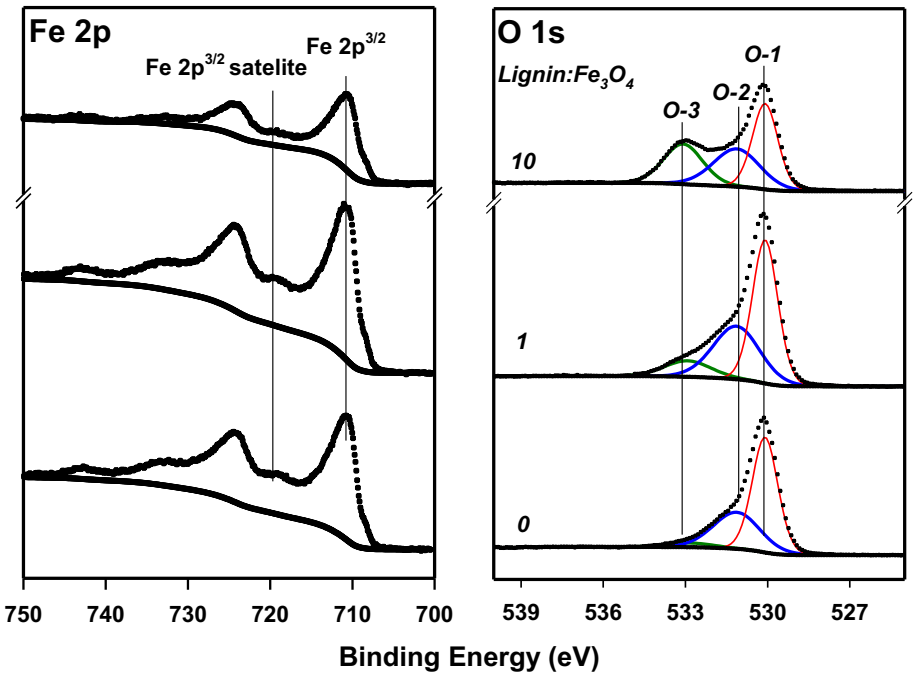

Fig. 3. Representative stackplots for the Fe 2p region and the fitted O 1s region for the lignin@Fe_3O_4 at different lignin:Fe_3O_4 mass ratios. Number labels represent lignin:Fe_3O_4 ratios. (right) The spectra for O1s (black) is fitted with three curves: O-1 for Fe—O (red), O-2 for contributions from both Fe_3O_4 and lignin (blue), and O-3 for lignin contributions (green). (For interpretation of the references to colour in this figure legend, the reader is referred to the web version of this article.)

Fig. 4A presents the surface elemental distribution as a function of lignin:Fe_3O_4 mass ratio. The Fe:O ratio decreased while the C:O ratio increased as a function of increased lignin:Fe_3O_4 mass ratio, confirming the lignin surface layer formation. At a lignin:Fe_3O_4 ratio of 5, the changes ceased and the carbon and iron levels reached a steady state. The distribution of surface oxygen functionality did change as initially shown in Fig. 3 and is plotted in Fig. 4B. Consistent with the Fe and the C signals, the *O-1* (Fe) decreased and *O-3*- (lignin) increased with increasing lignin:Fe_3O_4 mass ratio, respectively. The *O-2* varies only slightly with increasing mass ratio.

3.2. Lignin content assessment in lignin@Fe_3O_4 nanocomposites

TGA analysis was utilized to determine bound lignin content and thermal stability of the lignin@Fe_3O_4 nanocomposites. Fig. 5A shows the total percent weight loss for each of the nanocomposites prepared in this study. The lignin content on the fabricated nanocomposites was calculated using the weight percentage reported at 800 °C, as shown in Eq. (S1). Fig. 5A displays the lignin content for each lignin:Fe_3O_4 mass ratio analyzed in this study, which varied between 5% to 40% [Table S3 shows the calculated values]. An increase in the lignin content was observed as the lignin mass used in the preparation of the nanocomposites increased. In fact, at lignin:Fe_3O_4 mass ratios above 5:1, a one-way ANOVA fails at an $\alpha = 0.01$, suggesting that differences above the 5:1 mass ratio are not statistically significant. The general trend of the average lignin content can be represented as a logarithmic function, which is a similar trend to the results obtained for the FTIR (Fig. 1B).

Fig. 5B shows representative thermograms ran up to 850 °C. Moisture and residual solvent remained observed by the weight loss up to

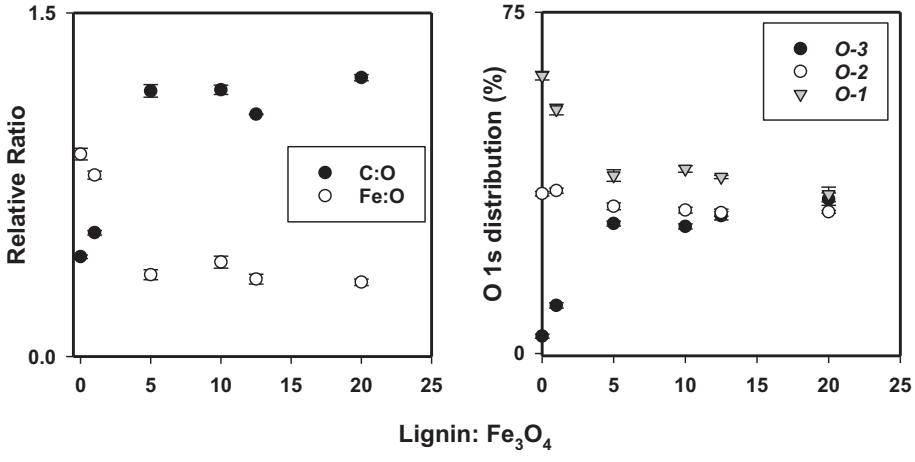

Fig. 4. XPS relative ratios (semi-quantitative) (A), and distribution of O 1s functionality for O—Fe (*O-1*), O—C (*O-2*), and O-lignin (*O-3*) bonds observed in high-resolution scans (B). [Data is representative of the average ± 1 standard deviation of 4 spatially unique measurements of one sample].

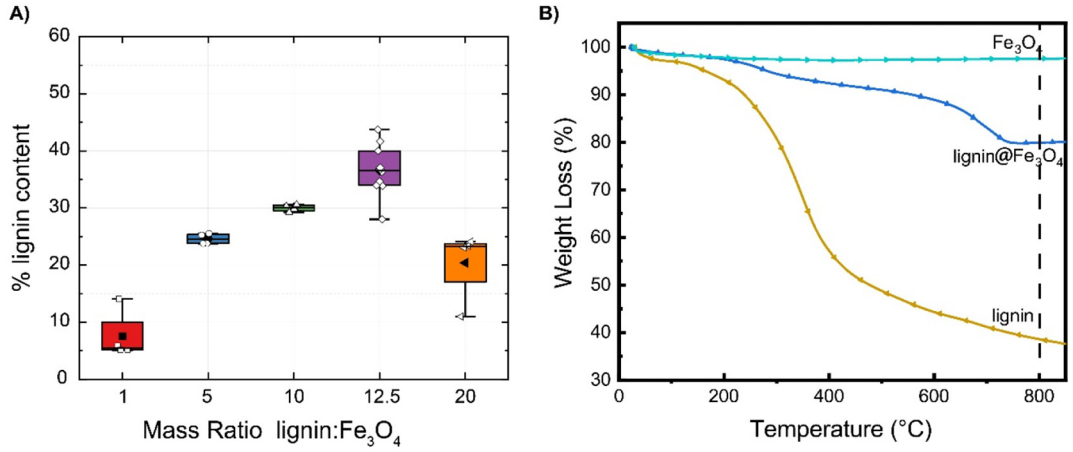

Fig. 5. A) Lignin percent content is shown for the various mass ratios of lignin@Fe_3O_4 nanocomposites. Average results of four samples are shown, each obtained in a different reaction (white dots), with the error bars representing one standard deviation. B) Representative TGA data for Fe_3O_4, 10:1 lignin@Fe3O4, and as-received lignin.

120 °C. After this temperature, the mass losses were attributed exclusively to the lignin content. Fe_3O_4 was stable and shows negligible weight changes up to 850 °C. Lignin, however, had almost a 65% weight loss at this temperature. Lignin@Fe_3O_4 nanocomposite had a lower weight loss with a similar trend compared to the neat lignin and Fe_3O_4 samples. For example, the 10:1 sample lost less than 30% of the initial weight at 850 °C (Fig. 5B), confirming improved thermal stability of the nanocomposites as compared to neat kraft lignin.

3.3. Morphological properties and particle size of lignin@Fe_3O_4 nanocomposites

TEM aided in identifying the morphology of the lignin@Fe_3O_4 nanocomposites prepared at different mass ratios. Fig. 6 shows each prepared lignin@Fe_3O_4 nanocomposite and the bare Fe_3O_4 nanoparticles as a control. These micrographs indicated that the lignin encapsulated the Fe_3O_4 particles, and upon drying, formed aggregated clusters. Based on the TEM analysis, the average size of the magnetic nanoparticles was 18.0 nm $\pm$ 4.8 nm for all the lignin@Fe_3O_4 prepared at the different lignin:Fe_3O_4 mass ratios (Fig. S4), which is comparable to the obtained XRD results. Previous studies have shown that kraft lignin can cause lignin networks agglomerates under alkaline conditions at low concentrations, resulting in fractal clusters [48], consistent with this study. Aggregated structures were observed at low lignin concentrations for the 1:1 lignin:Fe_3O_4 nanocomposites (Fig. 6B). As the lignin:Fe_3O_4 ratio increased, less agglomerates and more evenly dispersed nanoparticles with multiple nanoparticles encapsulated within a lignin shell (light contrast in TEM images) were observed

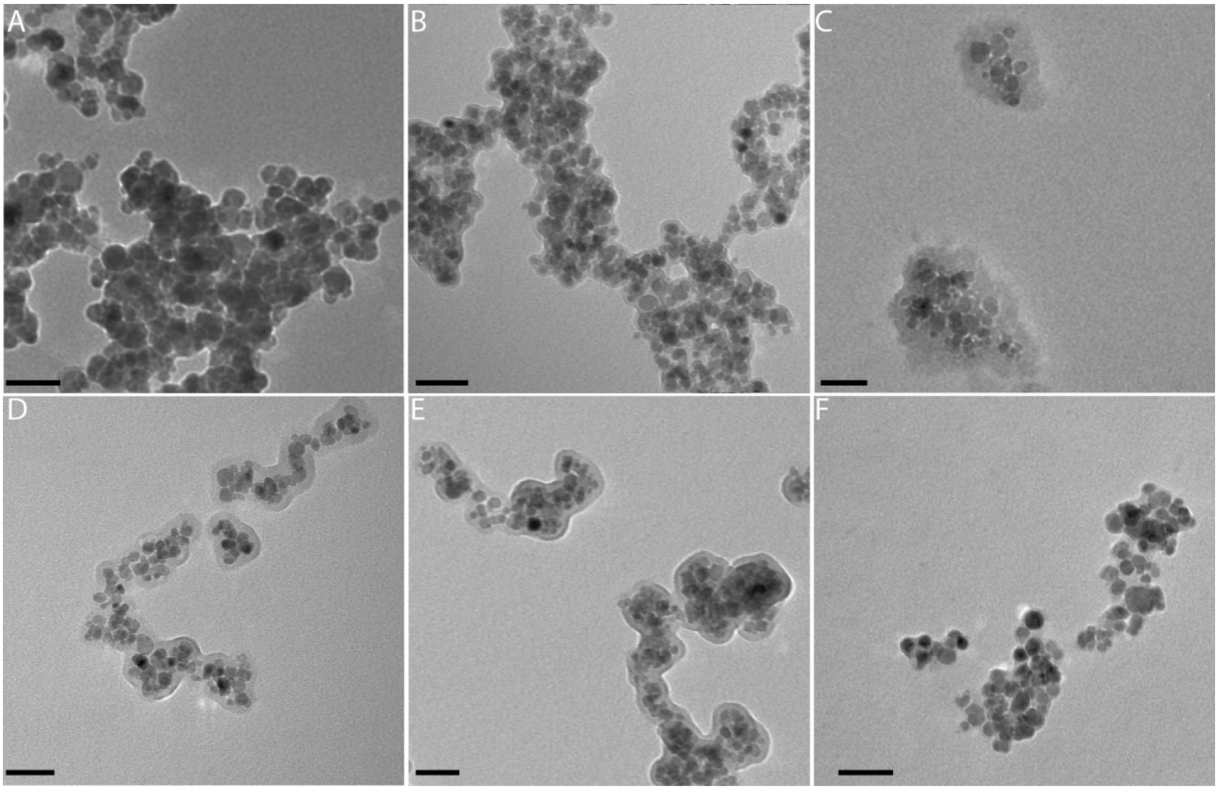

Fig. 6. TEM images of lignin@Fe_3O_4 nanocomposites and Fe_3O_4 nanoparticles. A is pristine Fe_3O_4, B is 1:1, C is 5:1, D is 10:1, E is 12.5:1, and F is 20:1 mass ratio of lignin to Fe_3O_4. For all the lignin@Fe_3O_4 samples, a lignin coating (lighter structure) around multiple magnetic nanoparticles (darker spheres) is observed. [Scale bar represents 50 nm].

(Fig. 6C–E). A thick coating of 7 nm to 14 nm was observed in the 10:1 and 12.5:1 samples (Fig. 6D and E) while a thin lignin corona layer (<5 nm) was observed for the 20:1 sample, suggesting that a large presence of kraft lignin during the pH precipitation does not enhance the lignin coating thickness. These results confirmed the presence of lignin and indicated a unique heterogeneous, multicore structure for the lignin@Fe_3O_4 nanocomposites prepared in this work for samples prepared at a minimum of 5:1 ratio.

The average hydrodynamic diameter measured using DLS was obtained for each lignin@Fe_3O_4 nanocomposite suspended in water (Fig. S5A). These results were used to determine if the reported particle size measured with DLS was affected by increasing the lignin:Fe_3O_4 mass ratios while suspended in water. Average hydrodynamic diameter was not consistent and varied from 129 nm to 182 nm. Also, a multimodal intensity plot was obtained for the lignin@Fe_3O_4 nanocomposites hydrodynamic diameter measurements (Fig. S5B). Possibly, this result could be due to the presence of heterogeneous nanostructures for the assembled nanoparticles. An additional comparison of the hydrodynamic diameter of the nanocomposites was performed using a Tukey test ($\alpha = 0.05$), revealing significant differences among the mean of most paired samples (Fig. S6). A one-way ANOVA test with an $\alpha = 0.05$ also confirmed that the means are significantly different. Despite these differences, the mean hydrodynamic diameter of each nanocomposite was stable, demonstrating that the lignin@Fe_3O_4 are suspended in water. TEM analysis revealed a multicore structure and the different diameters obtained through DLS for each nanocomposite could be attributed to the lignin content and assemblies in suspension, related to the fabrication and assembly process. ζ-potential measurements were performed to assess surface charge, indicating a constant value for all lignin@Fe_3O_4 nanoparticles at ca. −30 mV (Fig. S7). This result was slightly higher to the ζ-potential of the neat Fe_3O_4 (−40 mV) and closer to the lignin ζ-potential (−30 mV).

3.4. Magnetic study and separation of lignin@Fe_3O_4 nanocomposites from aqueous colloidal suspensions

Room temperature plots of the magnetic moment as a function of applied field M(H) measured with the SQUID instrument for neat Fe_3O_4 and various lignin:Fe_3O_4 mass ratios are shown in Fig. 7A. Uncoated Fe_3O_4 exhibited typical magnetization curve similar to the results reported by other groups [49], with low coercivity (<7958 A/m) and a saturation magnetization (Ms), of ≈64,000 $A \cdot m^2/kg^2$ which is comparable to previous literature values between 50,000 $A \cdot m^2/kg^2$ to 72,000 $A \cdot m^2/kg^2$ [22,50]. As the magnetic nanoparticles are coated with lignin, Ms. decreases due to the polymer coating contributing to the mass of the sample. Based on the saturation moment values, the amount of lignin coating in the samples with different mass ratios can be compared. The 1:1 ratio of lignin@Fe_3O_4 nanocomposite had similar M(H) results to uncoated Fe_3O_4 indicating little to no coating on the Fe_3O_4 particles. The other lignin@Fe_3O_4 nanocomposites showed a decrease in Ms. and are presumed to contain more lignin coating. Samples with mass ratios of 5:1, 10:1 and 20:1 have very similar magnetic saturation; (45,300, 45,200, and 46,600) $A \cdot m^2/kg^2$, respectively, implying that the coating amounts are also similar among these materials. These results showed a higher magnetization than other studies on lignin-coated Fe_3O_4 that reported 15,000 $A \cdot m^2/kg^2$ to 40,000 $A \cdot m^2/kg^2$ [22,25]. This magnetization study confirmed the lignin@Fe_3O_4 nanocomposites magnetic properties and further identified the lignin coating on the particles.

A preliminary adsorption test was performed using methylene blue (MB) and the prepared Lignin@Fe_3O_4 nanocomposites. UV–Vis absorbance was measured before and after the addition of the various ratios of lignin@Fe_3O_4 nanocomposites to determine the amount of MB adsorbed [Table S4]. All lignin@Fe_3O_4 nanocomposites removed at least 55% of the dye, demonstrating that these particles have the potential to be used as organic dye sorbents, which is consistent with the previous characterization results. For instance, the 1:1 lignin:Fe_3O_4 sample had a 55.6% ± 10.4% adsorption efficiency. This removal efficiency increased, reaching values as high as 74.1% ± 7.1% as the lignin:Fe_3O_4 content increased to 20:1. Variations in the adsorption efficiency also increased by increasing the mass ratio (Fig. 7B).

The maximum MB amount removed was 12.53 mg/g, demonstrating the potential of lignin@Fe_3O_4 nanocomposites sorbents that can be separated under the presence of an external magnetic field. Average adsorption capacities for samples with a lignin content at 10:1 or higher do not show significant MB adsorption efficiency changes (<10%), but the difference between the 1:1 to 10:1 is greater than 10%. Under this preliminary adsorption test, a one-way ANOVA test fails at $\alpha = 0.05$, suggesting no conclusive evidence of an adsorption performance enhancement based on the means for the five analyzed lignin:Fe_3O_4 samples. Future efforts should focus on obtaining a complete understanding of the sorption kinetics and performance of the lignin@Fe_3O_4 magnetic nanocomposites prepared and characterized in this work to remove dyes or other compounds of interest.

4. Conclusions

This work demonstrated a completely aqueous phase synthesis, based only on pH-driven precipitation, to prepare lignin@Fe_3O_4 nanocomposites using kraft lignin. We successfully fabricated core-shell

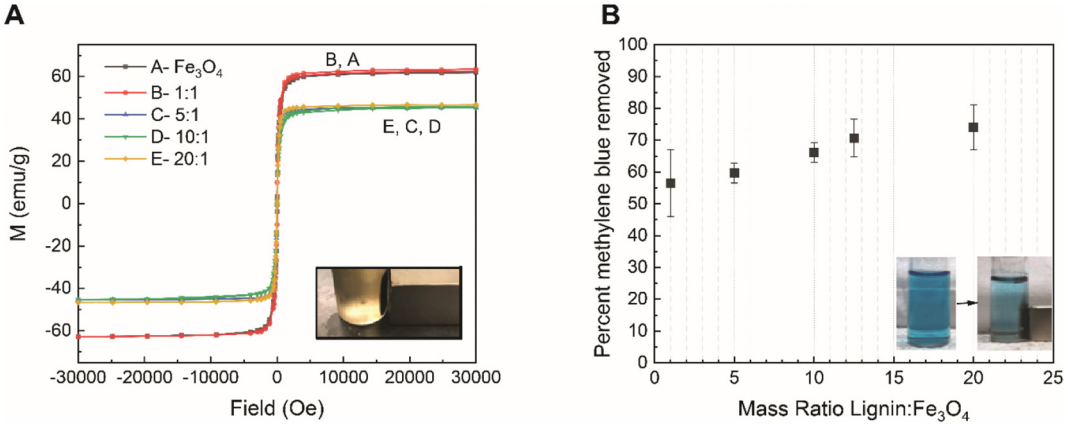

Fig. 7. A) Magnetization measurements of lignin@Fe_3O_4 nanocomposites (lignin:Fe_3O_4) and neat Fe_3O_4 at 300 K [inset shows the magnetic separation of 1:1 specimen in solution with the aid of an external magnet; results were obtained with a minimum of 50 mg for each sample]. B) Methylene Blue percent removed using lignin@Fe_3O_4 nanocomposites at the different lignin to Fe_3O_4 mass ratios [inset shows initial methylene blue magnetic separation with a 10:1 lignin:Fe_3O_4 sample; plotted values show the average and standard deviation of three samples]. (For interpretation of the references to colour in this figure legend, the reader is referred to the web version of this article.)

lignin@Fe_3O_4 nanostructures for lignin:Fe_3O_4 mass ratios greater than 5, and characterized the nanocomposites using TGA, FTIR, XPS, TEM, and SQUID. Lignin@Fe_3O_4 possessed a well-defined heterogeneous, multicore magnetic structure where kraft lignin acts as a shell, and multiple Fe_3O_4 magnetic nanoparticles cluster together, forming the core. A thick lignin shell ranged between 7 nm to 14 nm based on the lignin to Fe_3O_4 mass ratio. The nanocomposites had a magnetic saturation value of approximately 45,000 $A \cdot m^2/kg^2$ and a maximum 74.1% ± 7.1% methylene blue adsorption efficiency. The inherent magnetic and adsorptive properties of lignin@Fe_3O_4 multicore nanostructures show potential in adsorption or chemical separation processes induced by low-strength, rare-earth magnets. Moreover, the demonstrated methodology eliminates the need to functionalize lignin or use organic solvents to prepare nanocomposites. Ultimately, this pH-induced method can potentiate other nanomaterials encapsulation with a kraft lignin shell to fabricate numerous lignin-based nanocomposites.

Notes

The manuscript was written through contributions of all authors. All authors have given approval to the final version of the manuscript.

CRediT authorship contribution statement

Frankie Petrie: Conceptualization, Investigation, Visualization, Formal analysis, Writing - Original Draft. **Justin Gorham**: Investigation, Formal analysis, Resources, Visualization, Writing - Review & Editing. **Robert Busch**: Investigation, Formal analysis, Data Curation, Visualization, Writing- Review & Editing. **Serhiy Leontsev**: Formal analysis, Writing-Review & Editing. **Esteban Ureña-Benavides**: Writing - Review & Editing, Funding acquisition. **Erick Vasquez**: Conceptualization, Formal analysis, Resources, Data Curation, Visualization, Writing - Review & Editing, Supervision, Project administration, Funding acquisition.

Declaration of competing interest

None.

Acknowledgment

The authors would like to acknowledge equipment access granted by the NEST center and the Chemistry Department at the University of Dayton, and access to the SQUID instrument in the Nanosystems Laboratory at The Ohio State University.

Funding source

This research was funded by the National Science Foundation (CBET-1704897, CBET-1705331). Additional support for TEM access was provided by The School of Engineering at The University of Dayton.

Appendix A. Supplementary data

Supplementary data to this article can be found online at https://doi.org/10.1016/j.ijbiomac.2021.03.105.

References

[1] S. Gillet, M. Aguedo, L. Petitjean, A.R.C. Morais, A.M. Da Costa Lopes, R.M. Łukasik, P.T. Anastas, Lignin transformations for high value applications: towards targeted modifications using green chemistry, Green Chem. 19 (2017) 4200–4233, https://doi.org/10.1039/c7gc01479a.

[2] S.M. Roopan, An overview of natural renewable bio-polymer lignin towards nano and biotechnological applications, Int. J. Biol. Macromol. 103 (2017) 508–514, https://doi.org/10.1016/j.ijbiomac.2017.05.103.

[3] F.S. Chakar, A.J. Ragauskas, Review of current and future softwood kraft lignin process chemistry, Ind. Crop. Prod. (2004)https://doi.org/10.1016/j.indcrop.2004.04.016.

[4] G. Gellerstedt, Softwood kraft lignin: raw material for the future, Ind. Crop. Prod. 77 (2015) 845–854, https://doi.org/10.1016/j.indcrop.2015.09.040.

[5] A. Vishtal, A. Kraslawski, Challenges in industrial applications of technical lignins, BioResources. 6 (2011) 3547–3568, https://doi.org/10.15376/biores.6.3.3547-3568.

[6] E.D. Bartzoka, H. Lange, K. Thiel, C. Crestini, Coordination complexes and one-step assembly of lignin for versatile nanocapsule engineering, ACS Sustain. Chem. Eng. 4 (2016) 5194–5203, https://doi.org/10.1021/acssuschemeng.6b00904.

[7] F. Xiong, Y. Han, S. Wang, G. Li, T. Qin, Y. Chen, F. Chu, Preparation and formation mechanism of renewable lignin hollow nanospheres with a single hole by self-assembly, ACS Sustain. Chem. Eng. 5 (2017) 2273–2281, https://doi.org/10.1021/acssuschemeng.6b02585.

[8] T. Leskinen, J. Witos, J.J. Valle-Delgado, K. Lintinen, M. Kostiainen, S.K. Wiedmer, M. Österberg, M.-L. Mattinen, Adsorption of proteins on colloidal lignin particles for advanced biomaterials, Biomacromolecules 18 (2017) 2767–2776, https://doi.org/10.1021/acs.biomac.7b00676.

[9] M. Ago, B.L. Tardy, L. Wang, J. Guo, A. Khakalo, O.J. Rojas, Supramolecular assemblies of lignin into nano- and microparticles, MRS Bull. 42 (2017) 371–378, https://doi.org/10.1557/mrs.2017.88.

[10] M.B. Agustin, P.A. Penttilä, M. Lahtinen, K.S. Mikkonen, Rapid and direct preparation of lignin nanoparticles from alkaline pulping liquor by mild ultrasonication, ACS Sustain. Chem. Eng. 7 (2019) 19925–19934, https://doi.org/10.1021/acssuschemeng.9b05445.

[11] M.A. Adebayo, L.D.T. Prola, E.C. Lima, M.J. Puchana-Rosero, R. Cataluña, C. Saucier, C.S. Umpierres, J.C.P. Vaghetti, L.G. da Silva, R. Ruggiero, Adsorption of Procion Blue MX-R dye from aqueous solutions by lignin chemically modified with aluminium and manganese, J. Hazard. Mater. 268 (2014) 43–50, https://doi.org/10.1016/J.JHAZMAT.2014.01.005.

[12] Z.H. Liu, N. Hao, S. Shinde, M.L. Olson, S. Bhagia, J.R. Dunlap, K.C. Kao, X. Kang, A.J. Ragauskas, J.S. Yuan, Codesign of combinatorial organosolv pretreatment (COP) and lignin nanoparticles (LNPs) in biorefineries, ACS Sustain. Chem. Eng. 7 (2019) 2634–2647, https://doi.org/10.1021/acssuschemeng.8b05715.

[13] M. Ago, B. Tardy, L. Wang, J. Guo, A. Khakalo, O. Rojas, Supramolecular assemblies of lignin into nano- and microparticles, MRS Bull. 42 (2017) 371–378, https://doi.org/10.1557/mrs.2017.88.

[14] Y. Pang, S. Wang, X. Qiu, Y. Luo, H. Lou, J. Huang, Preparation of lignin/sodium dodecyl sulfate composite nanoparticles and their application in Pickering emulsion template-based microencapsulation, J. Agric. Food Chem. 65 (2017) 11011–11019, https://doi.org/10.1021/acs.jafc.7b03784.

[15] P.K. Mishra, A. Ekielski, A simple method to synthesize lignin nanoparticles, Colloids Interfaces 3 (2019) 52, https://doi.org/10.3390/colloids3020052.

[16] On the solution structure of kraft lignin in ethylene glycol and its implication for nanoparticle preparation, Nanoscale Adv. (2018)https://doi.org/10.1039/C8NA00042E.

[17] F. Zikeli, V. Vinciguerra, S. Sennato, G. Scarascia Mugnozza, M. Romagnoli, Preparation of lignin nanoparticles with entrapped essential oil as a bio-based biocide delivery system, ACS Omega 5 (2020) 358–368, https://doi.org/10.1021/acsomega.9b02793.

[18] H. Li, Y. Deng, B. Liu, Y. Ren, J. Liang, Y. Qian, X. Qiu, C. Li, D. Zheng, Preparation of nanocapsules via the self-assembly of kraft lignin: a totally green process with renewable resources, ACS Sustain. Chem. Eng. 4 (2016) 1946–1953, https://doi.org/10.1021/acssuschemeng.5b01066.

[19] Fabrication of environmentally biodegradable lignin nanoparticles, ChemPhysChem 13 (2012) 4235–4243, https://doi.org/10.1002/cphc.201200537.

[20] W. Wu, Z. Wu, T. Yu, C. Jiang, W.-S. Kim, Recent progress on magnetic iron oxide nanoparticles: synthesis, surface functional strategies and biomedical applications, Sci. Technol. Adv. Mater. 16 (2015), 023501, https://doi.org/10.1088/1468-6996/16/2/023501.

[21] J. Zdarta, K. Antecka, A. Jędrzak, K. Synoradzki, M. Łuczak, T. Jesionowski, Biopolymers conjugated with magnetite as support materials for trypsin immobilization and protein digestion, Colloids Surf. B: Biointerfaces 169 (2018) 118–125, https://doi.org/10.1016/J.COLSURFB.2018.05.018.

[22] Ł. Klapiszewski, J. Zdarta, K. Antecka, K. Synoradzki, K. Siwińska-Stefańska, D. Moszyński, T. Jesionowski, Magnetite nanoparticles conjugated with lignin: a physicochemical and magnetic study, Appl. Surf. Sci. 422 (2017) 94–103, https://doi.org/10.1016/J.APSUSC.2017.05.255.

[23] Ł. Klapiszewski, K. Siwińska-Stefańska, D. Kołodyńska, Development of lignin based multifunctional hybrid materials for Cu(II) and Cd(II) removal from the aqueous system, Chem. Eng. J. 330 (2017) 518–530, https://doi.org/10.1016/J.CEJ.2017.07.177.

[24] D. Kołodyńska, M. Gęca, I.V. Pylypchuk, Z. Hubicki, Development of new effective sorbents based on nanomagnetite, Nanoscale Res. Lett. 11 (2016), 152, https://doi.org/10.1186/s11671-016-1371-3.

[25] Y. Ma, D. Zheng, Z. Mo, R. Dong, X. Qiu, Magnetic lignin-based carbon nanoparticles and the adsorption for removal of methyl orange, Colloids Surfaces A Physicochem. Eng. Asp. 559 (2018) 226–234, https://doi.org/10.1016/J.COLSURFA.2018.09.054.

[26] B. Yu, A. Gele, L. Wang, Iron oxide/lignin-based hollow carbon nanofibers nanocomposite as an application electrode materials for supercapacitors, Int. J. Biol. Macromol. 118 (2018) 478–484, https://doi.org/10.1016/J.IJBIOMAC.2018.06.088.

[27] A. Jędrzak, T. Rębiś, M. Kuznowicz, T. Jesionowski, Bio-inspired magnetite/lignin/polydopamine-glucose oxidase biosensing nanoplatform. From synthesis, via sensing assays to comparison with others glucose testing techniques, Int. J. Biol. Macromol. 127 (2019) 677–682, https://doi.org/10.1016/j.ijbiomac.2019.02.008.

[28] T. Baran, I. Sargin, Green synthesis of a palladium nanocatalyst anchored on magnetic lignin-chitosan beads for synthesis of biaryls and aryl halide cyanation, Int. J. Biol. Macromol. 155 (2020) 814–822, https://doi.org/10.1016/j.ijbiomac.2020.04.003.

[29] M. Nasrollahzadeh, N.S.S. Bidgoli, Z. Issaabadi, Z. Ghavamifar, T. Baran, R. Luque, Hibiscus Rosasinensis L. aqueous extract-assisted valorization of lignin: preparation of magnetically reusable Pd NPs@Fe3O4-lignin for Cr(VI) reduction and Suzuki-Miyaura reaction in eco-friendly media, Int. J. Biol. Macromol. 148 (2020) 265–275, https://doi.org/10.1016/j.ijbiomac.2020.01.107.
[30] X. Zhang, Y. Li, Y. Hou, Preparation of magnetic polyethylenimine lignin and its adsorption of Pb(II), Int. J. Biol. Macromol. 141 (2019) 1102–1110, https://doi.org/10.1016/j.ijbiomac.2019.09.061.
[31] A. Hasan, P. Fatehi, Self-assembly of kraft lignin-acrylamide polymers, Colloids Surfaces A Physicochem. Eng. Asp. 572 (2019) 230–236, https://doi.org/10.1016/j.colsurfa.2019.04.002.
[32] X. Zhang, M. Yang, Q. Yuan, G. Cheng, Controlled preparation of corncob lignin nanoparticles and their size-dependent antioxidant properties: toward high value utilization of lignin, ACS Sustain. Chem. Eng. (2019)https://doi.org/10.1021/acssuschemeng.9b03535.
[33] E. Melro, A. Filipe, D. Sousa, A.J.M. Valente, A. Romano, F.E. Antunes, B. Medronho, Dissolution of kraft lignin in alkaline solutions, Int. J. Biol. Macromol. 148 (2020) 688–695, https://doi.org/10.1016/j.ijbiomac.2020.01.153.
[34] T.-J. Yoon, H. Lee, H. Shao, S. Hilderbrand, R. Weissleder, Multicore assemblies potentiate magnetic properties of biomagnetic nanoparticles, Adv. Mater. 23 (2011) 4793–4797, https://doi.org/10.1002/adma.201102948.
[35] R. Massart, Preparation of aqueous magnetic liquids in alkaline and acidic media, IEEE Trans. Magn. 17 (1981) 1247–1248, https://doi.org/10.1109/TMAG.1981.1061188.
[36] T. Fujii, F.C. Voogt, T. Hibma, G.A. Sawatzky, *In situ* XPS spectra of nonstoichiometric $Fe_{3-\delta}O_4$ (100) films, Surf. Sci. Spectra 6 (1999) 337–346, https://doi.org/10.1116/1.1247938.
[37] M.S. Kent, J. Zeng, N. Rader, I.C. Avina, C.T. Simoes, C.K. Brenden, M.L. Busse, J. Watt, N.H. Giron, T.M. Alam, M.D. Allendorf, B.A. Simmons, N.S. Bell, K.L. Sale, Efficient conversion of lignin into a water-soluble polymer by a chelator-mediated Fenton reaction: optimization of H_2O_2 use and performance as a dispersant, Green Chem. 20 (2018) 3024–3037, https://doi.org/10.1039/C7GC03459H.
[38] W. Yang, E. Fortunati, D. Gao, G.M. Balestra, G. Giovanale, X. He, L. Torre, J.M. Kenny, D. Puglia, Valorization of acid isolated high yield lignin nanoparticles as innovative antioxidant/antimicrobial organic materials, ACS Sustain. Chem. Eng. 6 (2018) 3502–3514, https://doi.org/10.1021/acssuschemeng.7b03782.
[39] Ł. Klapiszewski, K. Siwińska-Stefańska, D. Kołodyńska, Preparation and characterization of novel TiO2/lignin and TiO2-SiO2/lignin hybrids and their use as functional biosorbents for Pb(II), Chem. Eng. J. 314 (2017) 169–181, https://doi.org/10.1016/J.CEJ.2016.12.114.
[40] C. Yuan, Z. Lou, W. Wang, L. Yang, Y. Li, Synthesis of Fe3C@C from pyrolysis of Fe3O4-lignin clusters and its application for quick and sensitive detection of PrP Sc through a sandwich SPR detection assay, Int. J. Mol. Sci. 20 (2019)https://doi.org/10.3390/ijms20030741.
[41] I. Martínez-Mera, M.E. Espinosa-Pesqueira, R. Pérez-Hernández, J. Arenas-Alatorre, Synthesis of magnetite (Fe3O4) nanoparticles without surfactants at room temperature, Mater. Lett. 61 (2007) 4447–4451, https://doi.org/10.1016/J.MATLET.2007.02.018.
[42] S. Sun, H. Zen, Size-controlled synthesis of magnetite nanoparticles, J. Am. Chem. Soc. 124 (2002) 8204–8205, https://doi.org/10.1021/ja026501x.
[43] M. Yamaura, R. Camilo, L. Sampaio, M. Macêdo, M. Nakamura, H. Toma, Preparation and characterization of (3-aminopropyl)triethoxysilane-coated magnetite nanoparticles, J. Magn. Magn. Mater. 279 (2004) 210–217, https://doi.org/10.1016/J.JMMM.2004.01.094.
[44] M. Ma, Y. Zhang, W. Yu, H. Shen, H. Zhang, N. Gu, Preparation and characterization of magnetite nanoparticles coated by amino silane, Colloids Surfaces A Physicochem. Eng. Asp. 212 (2003) 219–226, https://doi.org/10.1016/S0927-7757(02)00305-9.
[45] A. Bee, R. Massart, S. Neveu, Synthesis of very fine maghemite particles, J. Magn. Magn. Mater. 149 (1995) 6–9, https://doi.org/10.1016/0304-8853(95)00317-7.
[46] A.P. Grosvenor, B.A. Kobe, M.C. Biesinger, N.S. McIntyre, Investigation of multiplet splitting of Fe 2p XPS spectra and bonding in iron compounds, Surf. Interface Anal. 36 (2004) 1564–1574, https://doi.org/10.1002/sia.1984.
[47] T. Fujii, F.M.F. de Groot, G.A. Sawatzky, F.C. Voogt, T. Hibma, K. Okada, *In situ* XPS analysis of various iron oxide films grown by NO2-assisted molecular-beam epitaxy, Phys. Rev. B 59 (1999) 3195–3202, https://doi.org/10.1103/PhysRevB.59.3195.
[48] W. Zhao, B. Simmons, S. Singh, A. Ragauskas, G. Cheng, From lignin association to nano-/micro-particle preparation: extracting higher value of lignin, Green Chem. 18 (2016) 5693–5700, https://doi.org/10.1039/C6GC01813K.
[49] A. Gholizadeh, A comparative study of physical properties in Fe_3O_4 nanoparticles prepared by coprecipitation and citrate methods, J. Am. Ceram. Soc. 100 (2017) 3577–3588, https://doi.org/10.1111/jace.14896.
[50] X. Li, Y. He, H. Sui, L. He, One-step fabrication of dual responsive lignin coated Fe_3O_4 nanoparticles for efficient removal of cationic and anionic dyes, Nanomaterials 8 (2018) 162, https://doi.org/10.3390/nano8030162.